evaluate the propagation properties of surface waves, IEEE Trans Antennas Propag 52 (2004), 1871–1878.
7. R. Lopez and W. Scott, Jr., Measurement of ground-penetrating radar antenna patterns using modulated scatterers, Proc SPIE 5794 (2005), 459–469.
8. K. Munoz and R. Zhougi, Improvement of probe response extraction using time domain gating for embedded modulated scatterer technique, Mater Eval 66 (2008), 1084–1090.
9. K. Munoz and R. Zhougi, Application of swept frequency measurements to the embedded modulated scatterer technique, In: Proceedings of the 3rd International Conference on Electromagnetic Near-Field, Characterization and Imaging, pp. 176–181, 2007.
10. K. Kim and W. Scott, Design of a resistively-loaded vee dipole for ultra-wideband ground-penetrating radar applications, IEEE Trans Antennas Propag 53 (2005), 2525–2532.

SUBSTRATE INTEGRATED WAVEGUIDE DUAL-STOPBAND FILTER

Mahbubeh Esmaeili and Jens Bornemann
Department of Electrical and Computer Engineering, University of Victoria, Victoria, BC V8W 3P6, Canada; Corresponding author: j.bornemann@ieee.org

Received 21 October 2013

ABSTRACT: *A dual-stopband filter in substrate integrated waveguide (SIW) technology is presented. The filter uses a uniform SIW transmission line loaded by three quarter-wavelength* H*-plane stubs spaced by quarter-wavelength sections. The two stopbands contain three transmission zeros (TZs) each and are located at center frequencies of 10 and 12.2 GHz with corresponding bandwidths of 360 and 500 MHz, respectively. The center frequency and bandwidth of the passband, separating the two stopbands, are 11.03 and 1.26 GHz. A capacitive post is used to improve the return loss of this passband and the location of its reflection zeros (RZs). The filter is prototyped and measured, and good agreement between measured and simulated results is obtained. The measured results confirm the predictions in terms of locations of TZs and RZs as well as passband return loss and stopband attenuation levels.* © 2014 Wiley Periodicals, Inc. Microwave Opt Technol Lett 56:1561–1563, 2014; View this article online at wileyonlinelibrary.com. DOI 10.1002/mop.28384

Key words: *bandstop filter; bandstop stub; substrate integrated waveguide*

1. INTRODUCTION

Due to their ability to reject unwanted frequency components, bandstop filters are one of the key elements in modern communication systems. To reject a double-sideband signal, a dual-stopband filter is a viable option, both in terms of filter weight and manufacturing cost.

A few articles reported dual-stopband filters. An analytic method for synthesizing such filters is introduced in [1]. Microstrip stepped-impedance resonators are used in [2] to create a dual-stopband filter with narrow bandwidth. Another narrowband filter based on defected microstrip technology is reported in [3]. Narrow multiple-stopband filters for suppression of interfering signals in UWB applications are introduced in [4]. A dual-stopband microstrip filter design with wider bandwidth is reported in [5] and allows each stopband to have two transmission zeros (TZs). Moreover, an *E*-plane waveguide dual-stopband filter using a finite number of coupled resonators is presented in [6]. Most of the dual-stopband filters are prototyped in microstrip technology [2–5] and have very narrow bandwidth [2–4].

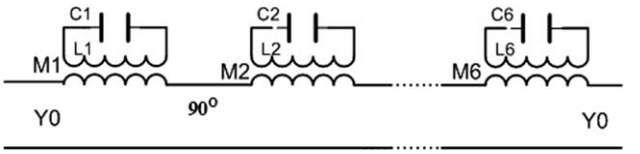

Figure 1 Equivalent lumped element circuit of the dual-stopband filter

Therefore, this article introduces a substrate integrated waveguide (SIW) dual-stopband filter with wider stopbands. The design uses three quarter-wavelength *H*-plane stubs spaced by quarter-wavelength SIW sections. A capacitive post is used to improve the return loss in the passband between the two stopbands.

2. DESIGN

Each bandstop resonator element is modeled by a shunt LC circuit as shown in Figure 1. For the design of a dual-stopband filter with three TZs in each stopband, we cascade six shunt LC circuits resonating at different center frequencies. All shunt LC circuits are separated by 90 degree transmission lines. An optimization process is applied to the equivalent circuit of Figure 1 to obtain two stopbands at center frequencies of 10 and 12.2 GHz with corresponding bandwidth of 360 and 500 MHz. While C_i and L_i determine the locations of TZs, coupling factors M_i determine the positions of reflection zeros (RZs) by scaling the total admittance of each shunt LC circuit by the factor M_i. Table 1 shows the final inductor, capacitor, and coupling values after optimization.

When implementing such a filter in SIW technology, it is found that the fundamental modes of the resonating stubs produce stopbands that are too wide to form highly selective stopband characteristics. Therefore, the first and second higher order modes of each resonating stub are used to create two stopbands with three TZs each. The fundamental-mode resonances occur close to the cutoff frequencies of the SIW input and output ports and thus are well below the frequency range for this filter design.

CST Microwave Studio is used to simulate a loaded uniform SIW line with three quarter-wavelength *H*-plane stubs spaced by quarter-wavelength sections, as shown in Figure 2(a). The diameters of all via holes are 1 mm. The substrate material is chosen as RT/Duroid 6002 with a relative permittivity of 2.94 and a relatively large thickness of 3.048 mm. This thickness is selected to accommodate a capacitive post that is inserted half-way into the SIW circuit, c.f. Figure 2(b), to improve the return loss of the passband located between the two stopbands. The diameter of the capacitive post equals that of the via holes. Note that microstrip-to-SIW transitions in Figure 2(a) are used to access the filter with measurement equipment. Their shapes differ from commonly used transitions because the 50 Ω microstrip line has wider line width due to the thick substrate used.

3. RESULTS

The frequency responses of the equivalent lumped element circuit and the circuit in Figure 2(a) as modeled in CST are

TABLE 1 Parameters Values of the Equivalent Lumped Element Circuit in Figure 1

i	C_i (pF)	L_i (pH)	M_i
1	5.3453	48.843	1.34
2	2.9866	84.814	1.35
3	2.6912	91.361	1.11
4	2.4443	72.569	0.90
5	1.7250	97.854	0.95
6	3.6488	44.644	0.88

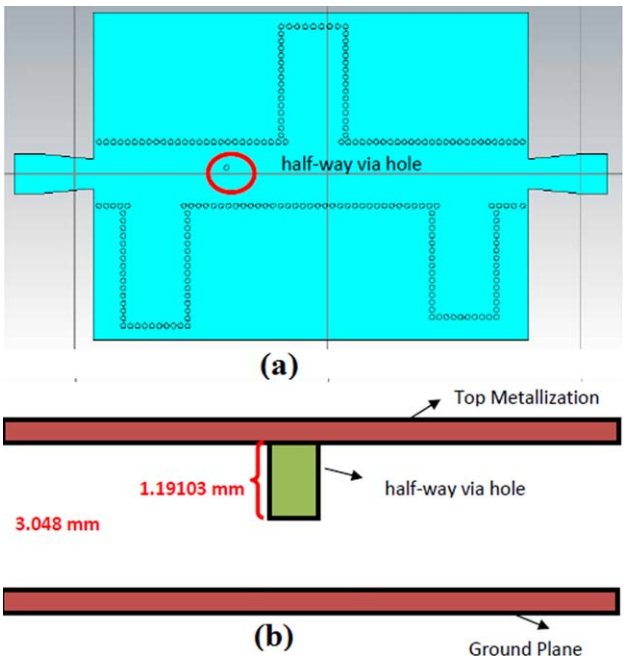

Figure 2 Dual-stopband SIW filter with half-way via hole; (a) top view of the filter and (b) side view of the half-way via hole. [Color figure can be viewed in the online issue, which is available at wileyonlinelibrary.com]

compared in Figure 3. The two stopbands and their TZs are well reproduced in the simulations. In the equivalent circuit, the waveguide sections, which separate the resonators, are assumed frequency-independent, and simple LC circuits (Fig. 1) are chosen to represent the resonators. However, the simulated results represent the full-wave and frequency-dependent response of the filter. Thus, some discrepancies between the simulated and equivalent circuits' results are observed, especially in the passband, as shown in Figure 3.

Figure 4 demonstrates the ability of the capacitive post to slightly improve the passband return loss. Note that the TZs in the two stopbands are not affected by this post.

The designed SIW dual-stopband filter is prototyped, and a photograph with all dimensions, including the position of the

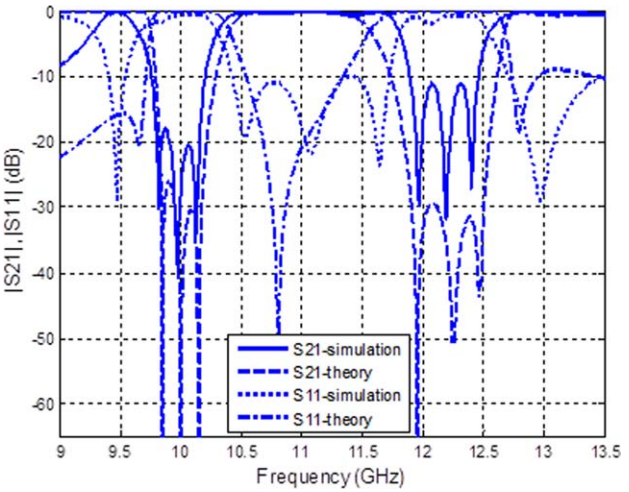

Figure 3 Comparison of scattering parameters of the dual-stopband filter between the equivalent circuit theory and simulations in CST. [Color figure can be viewed in the online issue, which is available at wileyonlinelibrary.com]

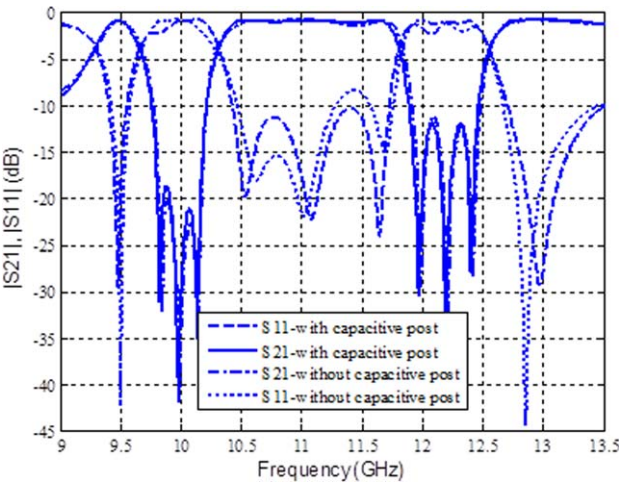

Figure 4 Simulated scattering parameters (CST) of the dual-stopband SIW filter with and without capacitive post. [Color figure can be viewed in the online issue, which is available at wileyonlinelibrary.com]

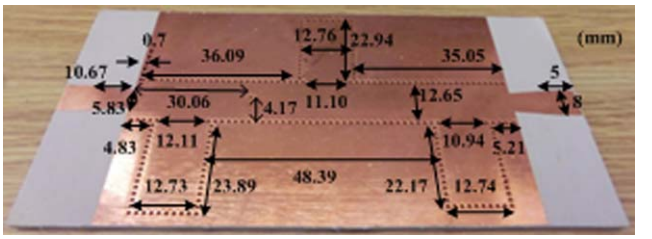

Figure 5 Photograph and dimensions of the fabricated dual-stopband filter in SIW technology. [Color figure can be viewed in the online issue, which is available at wileyonlinelibrary.com]

capacitive post, is depicted in Figure 5. For measurements, a Thru-Reflect-Line calibration kit is used to deembed the effects of coaxial connectors and microstrip-to-SIW transitions.

The measured and simulated performances are compared in Figure 6. It is observed that the experimental results reproduce the locations of TZs and RZs with good accuracy. The stopband center frequencies are located at 10 and 12.2 GHz and their

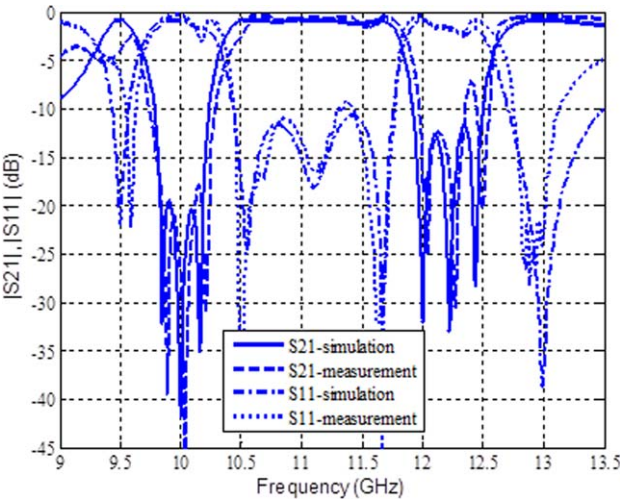

Figure 6 Comparison between measured and simulated scattering parameters. [Color figure can be viewed in the online issue, which is available at wileyonlinelibrary.com]

relatively wide bandwidths are 360 and 500 MHz, respectively. In addition, the attenuation in both stopbands as well as the passband return loss values are well represented in the measurements and agree well with simulations. Thus, the experimental results verify the simple design approach and give rise to filter designs involving multiple stopbands.

4. CONCLUSION

A dual-stopband SIW filter based on quarter-wavelength *H*-plane stubs is presented. The initial design uses six shunt LC circuits that are capable of producing three TZs in each stopband. The acceptable accuracy of the prototyped dual-stopband filter's response compared to that of simulations verifies the reliability of the design and demonstrates a viable option for dual-stopband filters in SIW technology.

REFERENCES

1. R.J. Cameron, M. Yu, and Y. Wang, Direct-coupled microwave filters with single and dual stopbands, IEEE Trans Microwave Theory Tech 53 (2005), 3288–3297.
2. K.S. Chin, J.H. Yeh, and S.H. Chao, Compact dual-band bandstop filters using stepped-impedance resonators, IEEE Microwave Wireless Compon Lett 17 (2007), 849–851.
3. J. Wang, H. Ning, Q. Xiong, M. Li, and L. Mao, A novel miniaturized dual-band bandstop filter using dual-plane defected structure, Prog Electromagn Res 134 (2013), 397–417.
4. K. Rambabu, M.Y. Chia, K.M. Chan, and J. Bornemann, Design of multiple-stopband filters for interference suppression in UWB applications, IEEE Trans Microwave Theory Tech 54 (2006), 3333–3338.
5. K.W. Wong, L. Chiu, and Q. Xue, A compact dual-band bandstop filter, Microwave Opt Technol Lett 51 (2009), 2952–2954.
6. R. Lopez-Villarroya and G. Goussetis, Novel topology for low-cost dual-band stopband filters, In: Proceedings of Asia-Pacific Microwave Conference, Singapore, 2009, pp. 933–936.

APERTURE COUPLED DUAL GROUND BACK FED S-SLOT RECTANGULAR MICROSTRIP ANTENNA FOR WIDE BAND OPERATION

N. K. Kulkarni and S. N. Mulgi
Department of PG Studies and Research in Applied Electronics, Gulbarga University, Gulbarga 585106, Karnataka, India;
Corresponding author: nag_kulb@rediffmail.com

Received 27 October 2013

ABSTRACT: *This article presents an aperture coupled dual ground back fed rectangular microstrip antenna for wideband operation. The bandwidth is enhanced by varying the width of S-shaped slot placed on the patch and the gap between the feed line on the ground plane of the antenna. The proposed antenna operates between 4 and 16 GHz of frequency range and gives a peak gain of 4.32 dB. The enhancement of bandwidth does not alter the nature of broadside radiation characteristics. The experimental and simulated results are in good agreement with each other. Design concepts of the antenna are given. The experimental results are presented and discussed. The proposed antennas may find applications in WiMax of IEEE802.16d, HIPERLAN/2 and radar communication systems.* © 2014 Wiley Periodicals, Inc. Microwave Opt Technol Lett 56:1563–1566, 2014; View this article online at wileyonlinelibrary.com. DOI 10.1002/mop.28383

Key words: *microstrip antenna; wideband; s-slot; aperture coupling; dual ground; back feed*

1. INTRODUCTION

In the present era, the rapidly growing wireless communication field has adopted various kinds of antennas for better communication. The microstrip antennas (MSAs) are attractive candidates for this field because of their excellent features such as planar, light weight, low profile, easy fabrication, compatibility with microwave and millimeter-wave integrated circuits, low production cost [1], and so forth. Modern communication systems such as WiMax, HIPERLAN/2, and radar communication [2], often need antennas possessing two or more independent frequency bands with wide bandwidth and adequate gain, which can make a single antenna to use for transmit/receive applications. Hence, it has become an interesting area for the MSA designers to meet these requirements. There are various techniques available in the literature to improve the bandwidth of the MSAs. Among them the prominent ones are, the use of materials with low relative permittivity, thicker substrates, use of matching networks, multiresonators, multilayer substrates and meandered ground plane, slot loading, stacked shorted patch, [3–8], and so forth. The methods available for enhancement of the gain of MSAs are use of parasitic patches and strips, use of left-handed meta-materials [9–11], and so forth. The proposed methods are effective at the cost of increase in the size and bulkiness of the antenna. The dual and triple band antennas are realized by cutting slots of different geometries like bow-tie, rectangular shape, and so forth, on the radiating patch [12–16]. In this study, a simple dual ground concept has been proposed to realize wide band operation of MSA. The effect of width of S-shaped slot and ground plane is studied for enhancing the bandwidth without changing the nature of radiation characteristics. This kind of study is found to be rare in the literature

2. DESIGNING

The proposed antennas are fabricated using low-cost glass epoxy substrate material of thickness $h = 1.66$ mm and dielectric constant $\varepsilon_r = 4.2$. The artwork of the antennas is sketched using computer software AUTO CAD to achieve better accuracy. The photolithography process is used to fabricate the antennas.

Figure 1 shows the top view geometry of aperture coupled dual ground back fed S-slot rectangular microstrip antenna (ABSRMSA). The antenna uses the substrate of area $A_{\mathrm{Sub}} \times B_{\mathrm{Sub}} = 50 \times 80$ mm. The rectangular radiating patch has its length L_{P} and width W_{P}. The ABSRMSA is designed using the relations,

$$L_{\mathrm{P}} = \frac{c}{2f_r\sqrt{\varepsilon_{\mathrm{e}}}} - 2\Delta l\,(\mathrm{cm}) \tag{1}$$

where c is the velocity of light in cm and f_r is the designed frequency in GHz.

ε_{e} is the effective dielectric constant and Δl is the extension length of the fringing field in mm. The Δl and ε_{e} are given by,

$$\Delta l = 0.412h\left(\frac{(\varepsilon_{\mathrm{e}}+0.3)\left(\frac{W}{h}+0.264\right)}{(\varepsilon_{\mathrm{e}}-0.258)\left(\frac{W}{h}+0.8\right)}\right)$$

and

$$\varepsilon_{\mathrm{e}} = \frac{\varepsilon_r+1}{2} + \frac{\varepsilon_r-1}{2}\left(1+12\frac{h}{W}\right)^{1/2}$$

$$W_{\mathrm{P}} = \frac{c}{2f_r}\sqrt{\frac{2}{\varepsilon_r+1}} \tag{2}$$

The radiating patch of ABSRMSA is etched on the top surface of substrate S_1 and the underneath copper area of S_1 is completely